

Aerodynamic Analyses and Database Development for Ares I Vehicle First Stage Separation

Bandu N. Pamadi,^{*} Jing Pei,[†] Jeremy T. Pinier,[‡] Scott D. Holland,[§] Peter F. Covell^{**}

NASA Langley Research Center, Hampton, VA 23681

Goetz H. Klopfer^{††}

NASA Ames Research Center, Moffett Field, CA 94035

This paper presents the aerodynamic analysis and database development for the first stage separation of the Ares I A106 Crew Launch Vehicle configuration. Separate databases were created for the first stage and upper stage. Each database consists of three components: isolated or free-stream coefficients, power-off proximity increments, and power-on proximity increments. The power-on database consists of three parts, all plumes firing at nominal conditions, the one booster deceleration motor out condition, and the one ullage settling motor out condition. The isolated and power-off incremental databases were developed using wind tunnel test data. The power-on proximity increments were developed using CFD solutions.

^{*}Ares I Aero Database Manager, Langley Ares Project Office, Senior Aerospace Engineer, Vehicle Analysis Branch, Systems Analysis and Concepts Directorate, Associate Fellow AIAA, Bandu.N.Pamadi@nasa.gov

[†]Aerospace Engineer, Vehicle Analysis Branch, Systems Analysis and Concepts Directorate, member AIAA, Jing.Pei-1@nasa.gov

[‡]Aerospace Engineer, Configuration Aerodynamics Branch, Senior Member AIAA, Jeremy.T.Pinier@nasa.gov

[§]Vehicle Integration Element Manager, Langley Ares Project Office, Senior Aerospace Engineer, Aerothermodynamics Branch, Associate Fellow AIAA, Scott.D.Holland@nasa.gov

^{**}Chief Engineer, Langley Ares Project Office, Senior Aerospace Engineer, Vehicle Analysis Branch, Systems Analysis and Concepts Directorate, Associate Fellow, AIAA, Peter.F.Covell@nasa.gov

^{††}Senior Aerospace Engineer, Modeling and Simulation Application Branch, NASA Advance Supercomputing Division, Exploration Systems Mission Directorate, Goetz.H.Klopfer@nasa.gov

Nomenclature

C_A	= axial force coefficient, axial force/ qS
ΔC_A	= incremental axial force coefficient
C_l	= rolling moment coefficient, rolling moment/ qSD
ΔC_l	= incremental rolling moment coefficient
C_m	= pitching moment coefficient, pitching moment/ qSD
ΔC_m	= incremental pitching moment coefficient
C_N	= normal force coefficient, normal force/ qS
ΔC_N	= incremental normal force coefficient
C_n	= yawing moment coefficient, yawing moment/ qSD
ΔC_n	= incremental yawing moment coefficient
C_p	= pressure coefficient
C_Y	= side force coefficient, side force/ qS
ΔC_Y	= incremental side force coefficient
D	= reference length, diameter of the cylindrical section of the first stage, in
M	= Mach number
q	= Dynamic pressure, lb/ft ²
R_{sep}	= radial separation distance, in, $\sqrt{(X_{sep})^2 + (Y_{sep})^2}$
S	= Reference area, $\pi D^2/4$, in ²
X_{sep}	= axial separation distance measured in upper stage coordinate system, in
Y_{sep}	= lateral separation distance measured in upper stage coordinate system, in
Z_{sep}	= vertical separation distance measured in upper stage coordinate system, in
α	= angle of attack, deg
α_T	= total angle of attack, deg
$\Delta\alpha$	= relative angle of attack of first stage, $\alpha_{FS} - \alpha_{US}$
β	= sideslip angle, deg
$\Delta\beta$	= relative sideslip angle of first stage, $\beta_{FS} - \beta_{US}$
κ	= radial angle locating the first stage with respect to upper stage, deg

Suffixes:

FS = first stage

US = upper stage

T = total, as in total angle of attack

I. Introduction

The Constellation Program was a key element of the National Aeronautics and Space Administration's (NASA) Vision for Space Exploration [1]. One of the primary elements of that program was the design and development of a crew launch vehicle (CLV) to launch the crew exploration vehicle (CEV) into low Earth orbit (LEO). The CLV was later named the Ares I. The Ares design and analyses cycle (ADAC) began in 2006, and the Ares I vehicle configuration gradually evolved with progression of ADAC activity. The preliminary design review of the Ares I was held in September 2008 with the critical design review scheduled for 2011 and the expectation that the Ares I would be operational by 2015. The first developmental test vehicle, the Ares I-X, was flown successfully on October 28, 2009. However, the Constellation Program was canceled in October 2010. At that time, the ADAC-3 was in progress with the vehicle configuration designated as A106. NASA Langley Research Center (LaRC) in partnership with NASA Marshall Space Flight Center (MSFC) and NASA Ames Research Center was involved in the aerodynamic characterization and database development activity for the A106 configuration. Reference 2 discusses the development of liftoff/transition and ascent databases for the A106 configuration. This paper discusses the development of the database for A106 first stage separation.

The Ares I is a multistage launch vehicle (Fig. 1). The first stage is a five-segment redesigned solid rocket motor (RSRMV), a derivative of the Space Shuttle four-segment solid rocket booster (SRB) and is being developed by ATK under contract with NASA. The second stage vehicle comprises the launch abort system (LAS), the crew module (CM), the service module (SM), the spacecraft adapter (SA), the upper stage propulsion elements such as liquid oxygen (LOX) and hydrogen (H₂) tanks and the J2-X engine. The combination of the LAS, the CM, the SM, and the SA is called the crew exploration vehicle (CEV), which is also known as Orion.

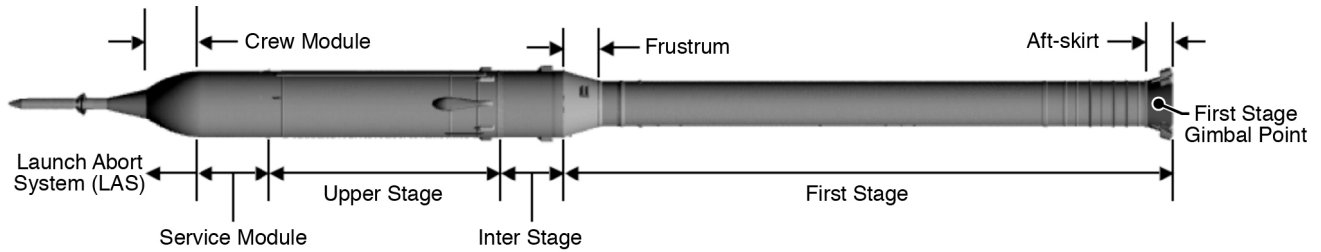


Fig. 1 Sketch of Ares I A106 vehicle showing major components of launch configuration.

The A106 configuration has 10 booster deceleration motors (BDMs) located on the aft-skirt of the first stage and four booster tumble motors (BTMs) contained in two pods (two motors in each pod) on the frustrum. Each BDM is the same as the Space Shuttle booster separation motor (BSM) used for SRB separation from the external tank/Orbiter. The BDMs are used to decelerate the first stage relative to the upper stage to aid axial separation. When the two stages are separated safely, the BTMs fire to put the first stage (with interstage attached) in a tumbling motion to dissipate energy and aid the parachute recovery. The first stage roll control system (RoCS) motors are located on the interstage and are used to balance the first stage combined aerodynamic rolling moment and the induced roll torque due to swirl and asymmetrical burning of the RSRMV. The upper stage reaction control motors (ReCS) are used for upper stage roll control subsequent to stage separation. All of the external structures, except the LAS nozzles, are usually referred to as protuberances. The umbilical between the CM and the SM, and the LH2 feedline fairing are two of the prominent protuberances on the A106 configuration. The major components and protuberances of the A106 configuration are shown in Fig. 1.

The nominal ascent trajectory for the International Space Station (ISS) mission is shown in Fig. 2. After liftoff/transition, the vehicle makes a gravity turn and follows a non-lifting ascent trajectory up to staging, which nominally occurs around Mach 5.7 and at an altitude of about 190,000 ft. However, in dispersed GNC7 (Guidance Navigation & Control cycle 7) simulations, the staging was found to occur anywhere from Mach 5 to 6 and at altitudes from 180,000 ft to 195,000 ft. The dynamic pressure ranges from 10 psf to 40 psf and the aerodynamic forces/moments during separation are small but not negligible. The first stage recovery process is similar to that of the Shuttle SRB. The LAS separation occurs at approximately at Mach 6.5 at an altitude of 200,000 ft. Subsequently, the CEV separates from the upper stage (without LAS) and continues its journey to the ISS. The rest of the upper stage disintegrates during its return to Earth, and it is not recovered.

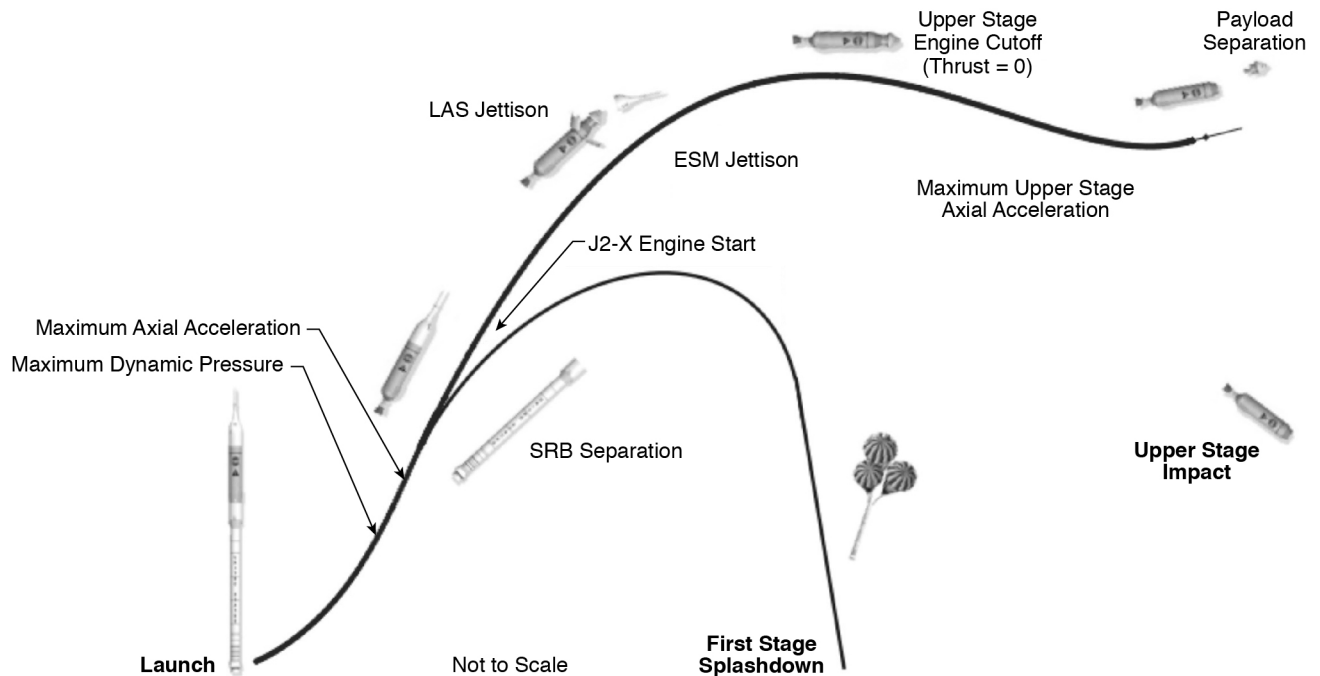


Fig. 2 Ares I A106 Crew Launch Vehicle nominal ascent trajectory.

The staging process is an in-line separation of the first stage from the upper stage exposing the J2-X engine and is possibly the most critical part of the Ares I CLV flight for a successful mission. Apollo/Saturn launch vehicles also had an in-line first stage separation [3]. At staging, the thrust of the first stage booster will be a small fraction of its initial value at liftoff and tails off to zero gradually. The start of separation is marked by the severance of the joint that connects the upper and the first stage. At that time, the four ullage settling motors (USMs) on the upper stage and the 10 BDMs on the first stage will have reached their full nominal thrust values. The J2-X engine thrust is very small until the first stage clears the J2-X nozzle. The stage separation is assumed to be complete after 2.5 sec when the axial separation between the two stages is about four RSRMV diameters. At this point, the tumble motors fire initiating first stage tumble and subsequent recovery.

The proximity aerodynamics is complex and challenging because of the presence of USM, BDM and J2-X plumes causing complex flow interactions in the upper stage base area and the first stage open cup region. It is equally challenging to design and fabricate small test models (typically 1% scale) simulating all the plumes and to obtain reliable test data for database development. The modern computational fluid dynamics (CFD) capability that was not available during the Apollo/Saturn and Space Shuttle development era is a viable option but it is difficult to validate CFD results in the absence of suitable test data.

The analysis and database discussed in this paper cover the separation event from start (mated condition) until the tumble motors fire. It consists of two parts, one for the first stage and the other for the upper stage. Each part consists of three components: (i) isolated freestream coefficients, (ii) power-off proximity increments with respect to isolated freestream coefficients, and (iii) power-on proximity increments with respect to power-off increments when all plumes are firing at their nominal thrust values. To meet Ares program requirements, the database also has two additional components, one BDM-out and one USM-out conditions. The one BDM-out and one USM-out databases, which provide increments with respect to all plumes firing nominally, were developed for each individual BDM and USM failure scenarios.

The isolated freestream and power-off incremental databases were developed using data from 1% scaled model stage separation tests in Arnold Engineering and Development Center (AEDC) Von Karman Facility (VKF) Tunnel A at Mach 5.5. Conducting power-on stage separation tests was outside the scope of this activity. All power-on proximity increments, including the one BDM out and one USM out cases, were estimated using OVERFLOW CFD solutions. A few selected CFD solutions were also obtained using LOCI-CHEM code.

II. Stage Separation Variables

During separation, the location of the first stage (FS) with respect to the upper stage (US) is defined through the separation reference point (SRP). The SRP is defined as the midpoint on the centerline of the fuselage station of the parting plane at separation. SRP_{FS} denotes the center of the separation plane on the FS, and SRP_{US} denotes the center of the separation plane on the US. By definition, SRP_{FS} and SRP_{US} are coincident prior to separation. Translational separation is defined as the location of SRP_{FS} relative to SRP_{US} in the upper stage coordinate system. The axial, lateral, and vertical displacements are defined as X_{sep} , Y_{sep} , and Z_{sep} , respectively. The angular orientation of the first stage with respect to the upper stage is defined by the relative angle of attack ($\Delta\alpha$) and sideslip angle ($\Delta\beta$). Figure 3 illustrates the nomenclature and the moment reference points used in the stage separation database. The upper stage moment reference center is located at the mid point of the separation plane and the first stage moment reference center at its gimbal point. The reference coordinate system used in Ares I aerodynamic database development activity is shown in Fig. 4.

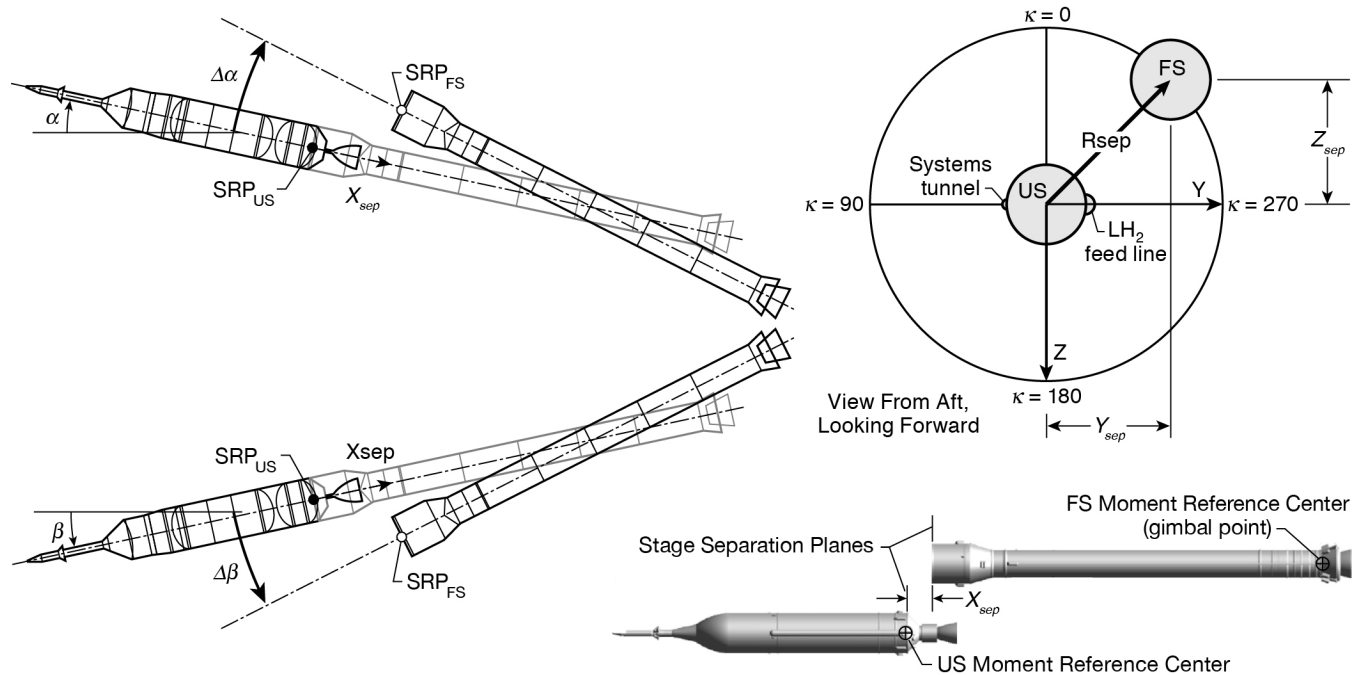


Fig. 3 Stage separation nomenclature.

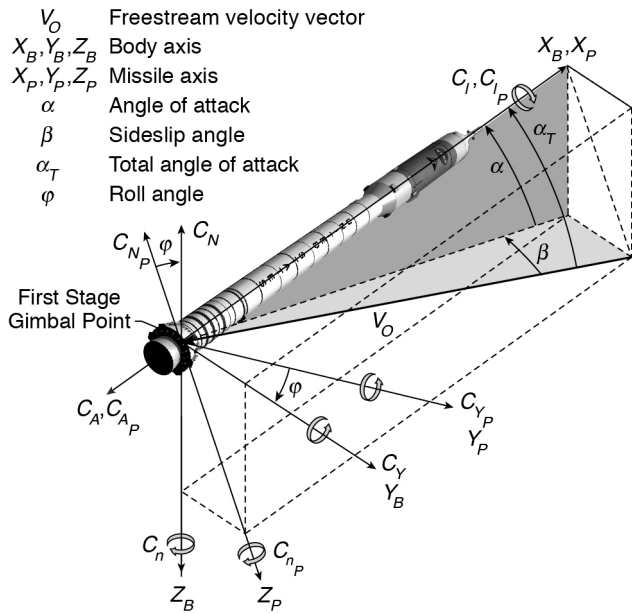


Fig. 4 Reference coordinate system.

III. Wind Tunnel Tests

The power-off stage separation tests were conducted at AEDC Von Karman Facility Tunnel A (VKF-A) during July 2008. At that time, the current Ares configuration was A103. The AEDC test was designated as Test VA-482 and was conducted on 1% A103 scale model at Mach 5.5 using the captive trajectory system (CTS). The CTS rig permitted positioning the first stage relative to the upper stage for all required combinations of translational and rotational orientations.

The database was developed using test data on clean axially symmetric models (no protuberances). However, the upper stage model is not perfectly axially symmetrical because it includes the LAS. The isolated (free-stream) database was developed using test data on first stage and upper stage in isolation, and the power-off proximity incremental database was developed using data from tests conducted with both stages in close proximity. Some limited test data were acquired on A103 test models with protuberances, and these data were used to estimate uncertainty.

Figure 5 illustrates the test setup. The upper stage was blade mounted, which allowed it to be pitched in the vertical plane. The first stage was sting mounted, which allowed both translational and rotational motion relative to the upper stage. Figure 6 illustrates the nozzle position relative to the cup when the upper stage is at a relative angle of attack with respect to the first stage.

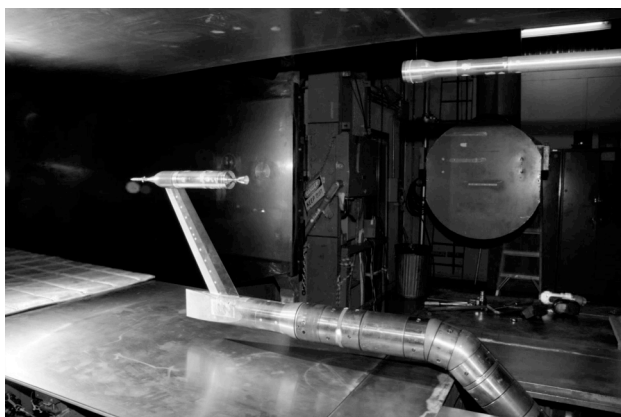


Fig. 5 Test model in AEDC VKF Tunnel A.

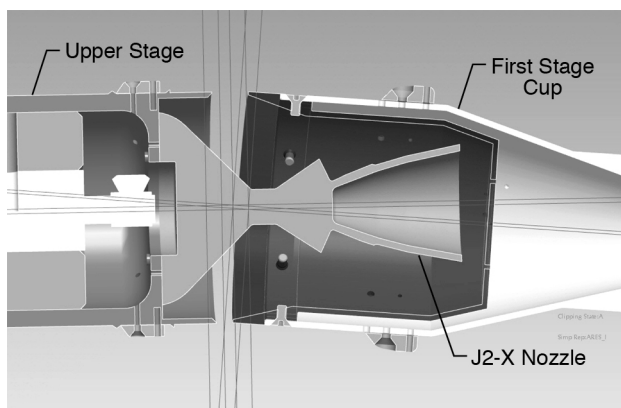


Fig. 6 J2-X nozzle and first stage cup positions during stage separation.

The power-off test matrix was developed to cover the dispersed separation trajectories. The test matrix had to be developed in advance because the CTS system needs to be preprogrammed before the commencement of each test. In view of this, it was necessary to ensure that no physical contact occurred between the first stage and upper stage models at any location in the test matrix particularly when the two models were in very close proximity. A collision detection code in MATLAB was developed to determine the closest possible locations without collision. The total air-on occupancy hours for Ares I stage separation tests in AEDC VKF Tunnel A were about 130.

In AEDC tests, the lateral location of the FS with respect to US was identified by radial (R_{sep}) and angular (κ) locations instead of Y_{sep} and Z_{sep} (Figure 3). There are six independent variables in the power-off AEDC stage separation test data given in Table I. During the tests, the upper stage remained stationary at a given angle of attack.

The first stage was set to the desired $\Delta\alpha$, $\Delta\beta$, R_{sep} , and κ . Then, the CTS rig traversed it to all the preprogrammed axial (X_{sep}) locations in the test matrix for that combination of test variables.

Table I Range of Variables for Power-off Stage Separation Tests

$\alpha_{T, US}$, deg	$\Delta\alpha$, deg	$\Delta\beta$, deg	X_{sep}/D	R_{sep}/D	κ
0, 5, 10	-5, 0, 5	-5, 0, 5	0.1 to 10.0	0 to 2.0	0 to 360 deg

The majority of the test data were taken at small X_{sep}/D and R_{sep}/D locations where the mutual interference effects between the two stages are expected to be largest. Figure 7 presents a schematic illustration of the test matrix data points for $\Delta\alpha = \Delta\beta = 0$, and Fig. 8 has sample Schlieren images of the flow field during separation. No test data were acquired when the upper stage was at nonzero sideslip angles. Reference 4 has available additional details of AEDC tests.

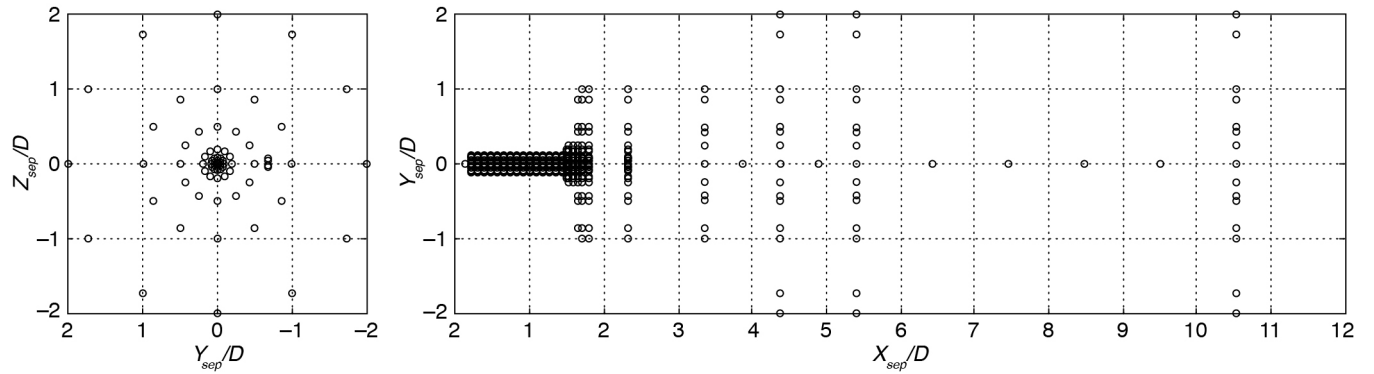


Fig. 7 Schematic illustration of AEDC test matrix for upper stage angles of attack of 0 and 5 degrees.

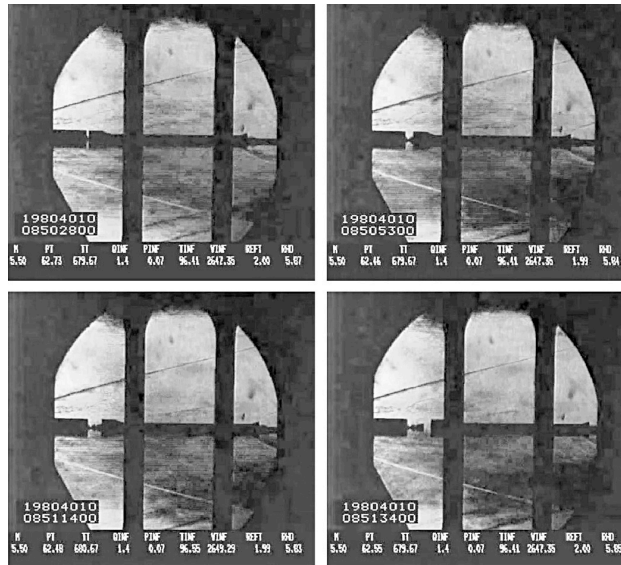


Fig. 8 Sample Schlieren images.

IV. CFD Solutions

The power-on incremental database was generated using the OVERFLOW CFD code [5]. Some selected CFD solutions were obtained using the LOCI-CHEM code [6] for perfect gas conditions for code-to-code comparisons and uncertainty estimation. The configuration used in the computations was the A106+ (also designated as A106p) configuration with all protuberances and 10 BDMs located at the mid location on the aft skirt. The A106+ configuration also provided definition of internal nozzle contour, the thrust cone, and J2-X thermal blanket as well as updated clocking of the BTMs.

Figure 9 shows the BDM and USM numbering. The Patrick 63 atmospheric model [7] was used to estimate free-stream static pressure, density, and temperature for input to CFD solutions. To calculate the power-on incremental coefficients, pairs of CFD solutions, one for power-on and the other for power-off, for identical flow conditions were generated. The majority of the CFD solutions were generated at nominal separation conditions.

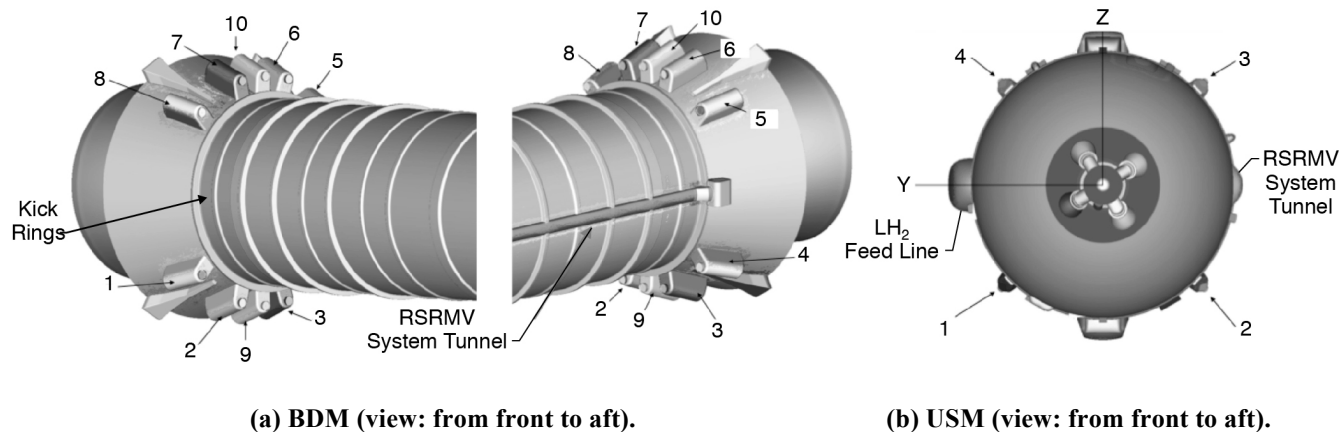


Fig. 9 BDM and USM nomenclature.

The USM, BDM, RSRMV and J2-X plumes and their firing schedules and thrust profiles were modeled using GNC7 input data. Figure 10 shows a plot of the nominal thrust profiles. The USM thrust varied very little during the 2.5 sec duration of separation event. The BDM thrust reached its peak value between 0 and 0.4 seconds and then tailed off rapidly. The RSRMV thrust tailed off gradually. The J2-X thrust was essentially zero at the start of separation but slowly built up as shown. The LAS, RoCS, and ReCS plumes were not modeled in CFD solutions. These time-based, nominal thrust profiles were tied to X_{sep}/D via the GNC7 nominal separation time history.

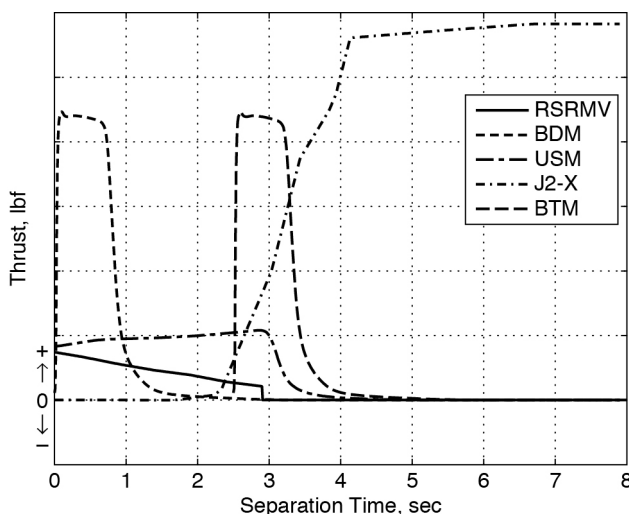
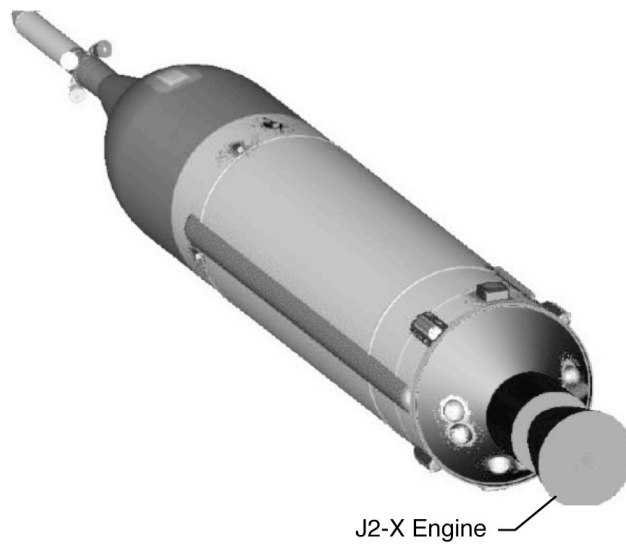
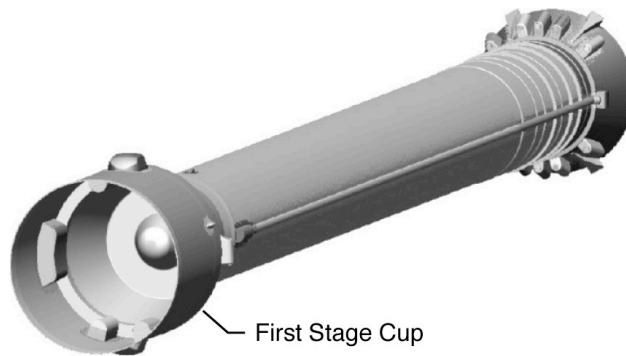


Fig. 10 Total thrust time histories.

OVERFLOW is a structured grid Navier-Stokes flow solver [8] using overset grids or zones to handle the complex geometry involved with the A106p configuration. Figure 11 shows the first and upper stage surface definitions for this configuration. Figure 12(a) shows the overset grid system used for A106p, and Fig. 12(b) shows a close up of the region around the J2-X nozzle and the first stage cup. A typical grid system for these computations consists of about 200 zones and a total of about 260 million grid points. To ensure that the CFD solutions were grid independent, overset grid best practices were followed [9]. In addition, to ensure that the physics of the plume effects applicable for stage separation aerodynamics were accurately modeled, plume validation studies were carried out as reported in reference. 10. It was not possible to obtain experimental data for the plume effects with the A106p configuration to use for CFD code validation.

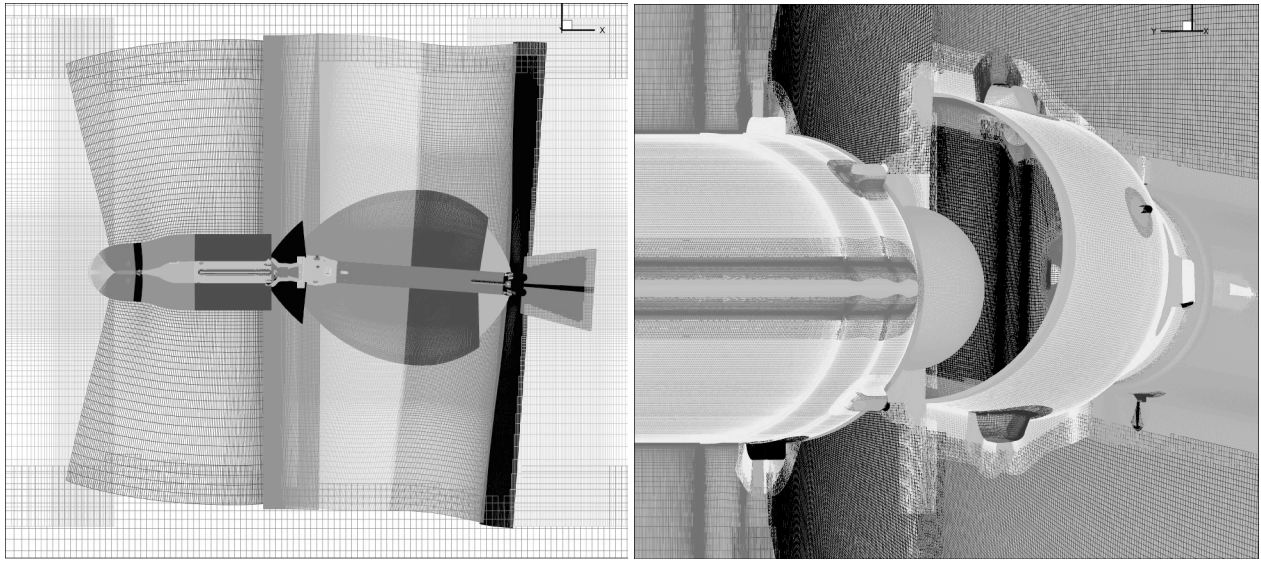


(a) Upper stage.



(b) First stage.

Fig. 11 Surface definitions used in OVERFLOW CFD computations.



(a) A106 overset grid system.

(b) J2-X nozzle and first-stage cup area.

Figure 12. Overset grid system used in OVERFLOW CFD computations.

An estimated 35 million CPU hours on the Pleiades computer system at NASA Ames Research Center were needed for: 120 solutions for power-on (60 each for plume-on and plume-of), 26 for BDM-out, and 16 for USM-out cases.

Figure 13 shows the flow field Mach and surface pressure contours at $X_{sep}/D = 0.1$ for power-off (no plumes) and power-on (all plumes at nominal conditions). Figure 14 shows the flow field in the J2-X nozzle and first stage cup for $X_{sep}/D = 0.6$. Figure 15 shows the flow field in the aft skirt region for BDM #10 failure. Note that C_p (pressure coefficient) contours show surface pressure distribution. Complete details of CFD work are available in reference 7.

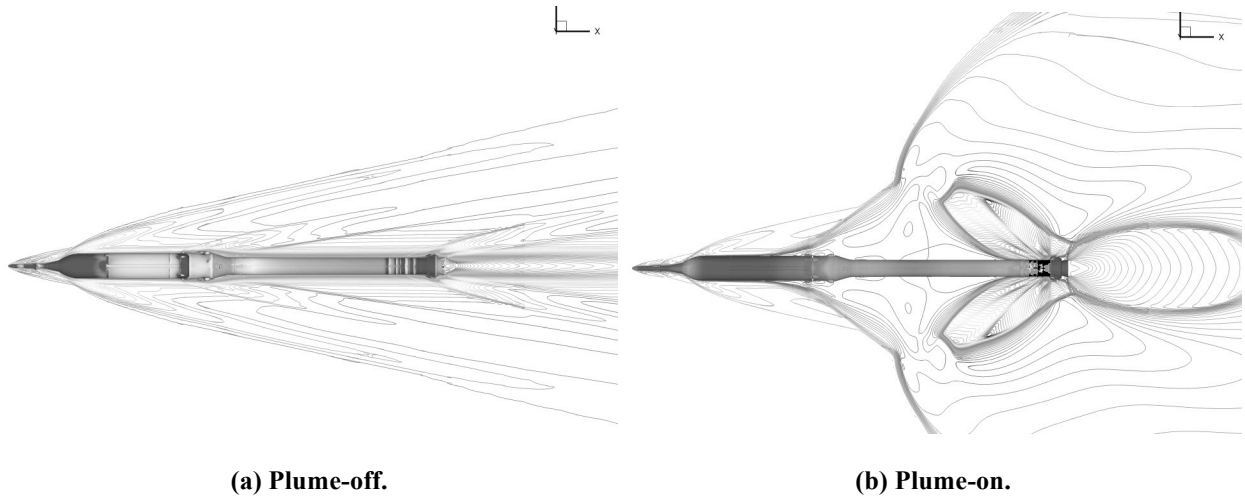


Fig. 13 Mach and surface pressure contours, $\alpha = 0$, $\Delta\alpha = 0$, $\Delta\beta = 0$, $R_{sep}/D = 0$, $X_{sep}/D = 0.1$ ($Y = 0$ plane).

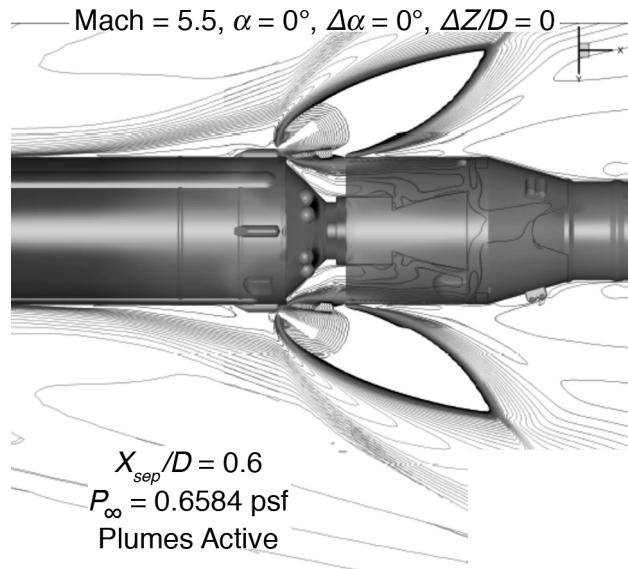


Fig. 14 Mach and surface pressure contours around the J2-X and the first stage cup region, $M = 5.5$,

$X_{sep}/D = 0.6$, $\alpha = 0$, $\Delta\alpha = 0$ and $Z_{sep}/D = 0$.

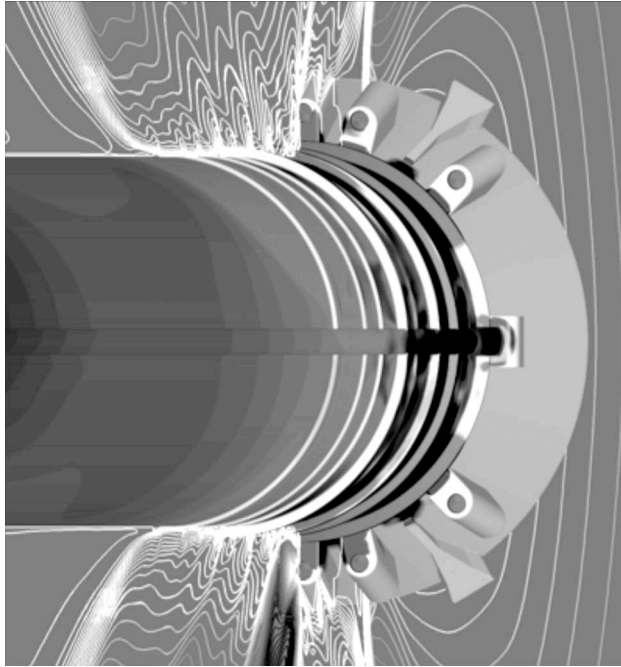


Fig. 15 Mach and surface pressure contours in aft-skirt area for BDM #10 failure case.

V. Database Development

All the aerodynamic coefficients in the database are provided in the body axis system. The methods and procedures used for each database are discussed in the following:

A. Isolated (Free-stream) Database

The AEDC test data on upper stage and first stage in isolation were used to develop this database. This database consists of six (6 DOF) aerodynamic coefficients (C_N , C_A , C_Y , C_m , C_l , C_n) for both upper stage and first stage as functions of angle of attack and sideslip.

B. Power-off Database

The power-off database provides incremental coefficients with respect to isolated coefficients to account for mutual aerodynamic interference effects of the first stage and upper stage in proximity for plume-off conditions. The power-off database was developed using AEDC test data on A103 clean configuration (no protuberances). The A106 clean configuration was very close to the A103 clean configuration. In view of this, this database is assumed to be applicable for A106 configuration. However, there were some differences in protuberances between A103 and A106. It was assumed that the influence of these protuberances is negligible on the proximity aerodynamic coefficients.

The power-off incremental coefficients were calculated by subtracting the isolated (free-stream) coefficients from the proximity coefficients for corresponding angle of attack/sideslip. The database consists of six force and moment increment coefficients (ΔC_N , ΔC_A , ΔC_Y , ΔC_m , ΔC_l , ΔC_n) for both the first stage and the upper stage. This 6 DOF database has six independent variables X_{sep}/D , R_{sep}/D , κ , $\alpha_{T,US}$, $\Delta\alpha$, and $\Delta\beta$. That is, each of the six power-off incremental coefficients of the upper stage and the first stage depend on these six independent variables.

The test data covered the following range of variables: $X_{sep}/D = 0$ to 10, $R_{sep}/D = 0$ to 2.0, upper stage angle of attack, $\alpha = 0, 5$ and 10 degrees. Because the upper stage was axially symmetrical, $\alpha = \alpha_{T,US}$. For each of the three values of α , the first stage relative angles of attack ($\Delta\alpha$) were 0 and ± 5 degrees and relative sideslip ($\Delta\beta$), 0 and ± 5 degrees. That is, for each α , there were nine combinations of $\Delta\alpha$ and $\Delta\beta$ for a total of 27 data sets. Since the test models were axially symmetric (except for the upper stage LAS nozzles), the upper stage can be assumed to be at total angles of attack of 0, 5, and 10 degrees. With this assumption, the power-off incremental coefficients when the upper stage was at a combined angle of attack and sideslip (such that total alpha was below 10 degrees) can be deduced using the available database.

The database was populated at selected break points in X_{sep}/D , R_{sep}/D and κ using multi-dimensional linear interpolation. Even though the CTS rig was preprogrammed to take data at specified X_{sep}/D , R_{sep}/D and κ , the actual values of these variables were slightly different. The GNC7 trajectories indicated that around 1.5 sec from separation initiation, when X_{sep}/D was approximately 1.914, the first stage cup clears the J2-X nozzle. After 2.5 seconds, when the two stages were about 4.25D apart, the tumble motors fired and the stage separation database discussed in this paper was no longer applicable. Hence, the power-off database was truncated at $X_{sep}/D = 5.4$, which was the next closest break point in the AEDC test matrix.

C. Power-on Database

This database accounts for plume interference effects. It has three parts: (1) all motors firing at their nominal thrust values, (2) one BDM-out, others firing nominally, and (3) one USM-out, others firing nominally. These three databases were generated using CFD solutions as discussed earlier.

1. All-Plumes Nominal Firing Database

The all plumes nominal firing database is an increment relative to the power-off database, that is, free-stream coefficients plus power-off increments. The pairs of OVERFLOW CFD solutions for all plumes firing nominally and

power-off for identical flow conditions were used to calculate these increments. These CFD solutions covered variations in X_{sep}/D , α , β , $\Delta\alpha$, $\Delta\beta$, and Δz . The variations in Δy were not considered. The power-off OVERFLOW solutions compared well with AEDC proximity test data. However, the power-on CFD solutions could not be validated because suitable test data were not available. Performing power-on stage separation tests was outside of the scope of this activity.

The available CFD solutions (60 each for power-off and power-on, total 120) were not adequate to develop a detailed six dimensional database. The GNC7 dispersed separation trajectories indicated that the variations in α , β , $\Delta\alpha$, $\Delta\beta$, Δy , and Δz from their nominal separation values (which are all close to zero) were really small. Therefore, it was decided to develop a simple, one-dimensional model with X_{sep}/D as the only variable and include all variations due to the rest of the variables in the uncertainty estimation. Thus, for a given X_{sep}/D , the data in the database were the mean values of the incremental coefficients for various α , β , $\Delta\alpha$, $\Delta\beta$, and R_{sep}/D at that X_{sep}/D . The differences between the mean values and the actual CFD increments were used to estimate uncertainty as discussed later. All incremental coefficients other than axial force increments were very small. Therefore, they were set to zero for both the first stage and the upper stage, and residuals were included in uncertainty.

2. *One BDM Out Database*

This database provides thrust based incremental coefficients for one BDM failure with respect to all plumes firing at the nominal conditions database. A total of nine CFD solutions were available for BDM #9, #10, #1, #4, and #5 out at various α and β for $X_{sep}/D = 0.1$. Variations in Δy and Δz were not included in BDM-out CFD solutions. The BDM-out increments were computed by subtracting all plumes nominally firing coefficients from the corresponding one BDM-out coefficients. The incremental coefficients for other values of X_{sep}/D were obtained by scaling these incremental coefficients by the BDM thrust ratio at that axial location. The BDM-out database includes effects of α and β . The first stage axial force and rolling moment increments coefficients were independent of which BDM had failed because of symmetry. All the upper stage incremental coefficients were set to zero because they were negligible.

3. *One USM-out Database*

This database provides thrust based incremental coefficients for a one USM failure with respect to an all plumes firing at nominal conditions database. A total of eight CFD solutions were available for USM #2 and #4 out at $X_{sep}/D = 0.1, 0.6, 1.0, \text{ and } 2.0$ and for α and β values of 0 and 4, with $\Delta\alpha = 0$ and $\Delta\beta = 0$. Variations in Δy and Δz were

not included in USM-out CFD solutions. The data for USM #1 and #3 were generated assuming symmetry. The USM-out increments were computed by subtracting all plumes nominally firing coefficients from the corresponding one USM-out coefficients. The nominal database was generated for $\alpha = \beta = 0$. The effects of α , β , $\Delta\alpha$, and $\Delta\beta$ were included in uncertainty estimation.

D. Uncertainty Estimation:

Isolated (Free-Stream) and Power-Off Database: The uncertainty in isolated (free-stream) coefficients and power-off incremental coefficients arose because of test data repeatability, measurement errors in the test data, errors due to flow/model asymmetry, and protuberance effects not included in the wind tunnel test models. The total uncertainty was obtained by the root-sum-square of these three components.

Power-On Database:

All plumes nominal firing database: Since sufficient information was not available to quantify uncertainty, the dispersion bounds were estimated based on engineering judgment. These dispersion bounds accounted for variations due to α , β , $\Delta\alpha$, $\Delta\beta$, and Δz not being included in the database and CFD modeling errors. These two sources of error were to be dispersed independently in GN&C simulations.

The dispersion bounds to account for α , β , $\Delta\alpha$, $\Delta\beta$, and Δz variations (Dispersion 1) were derived using the residuals obtained by subtracting the actual power-on CFD increments from the corresponding database values. For coefficients other than pitching and yawing moment, the maximum absolute values of the residuals were set as the dispersion bounds. For pitching and yawing moment incremental coefficients, dispersion bounds were first estimated at the vehicle center of gravity (CG). Then, the data were transferred back to the moment reference centers for each stage. This approach was taken to ensure that uncertainties in pitching and yawing moment incremental coefficients were properly implemented in simulations where the forces/moments are ultimately applied at the vehicle center of gravity. These bounds were further increased by 10 percent to account for unknown factors (such as Δy effect) and off-nominal flight conditions.

The CFD modeling errors (Dispersion 2) were estimated using available OVERFLOW and LOCI-CHEM perfect gas computations. The power-on increments for each of these two CFD codes were calculated by subtracting

the respective power-off coefficients. The dispersion bounds were set 30% higher than the maximum absolute differences to account for unknown factors such as CFD validation errors.

BDM-out dispersions: The BDM-out dispersion bounds consisted of two components: CFD modeling errors and variations due to off-nominal flight conditions. These two components were to be independently dispersed in simulations. Similar to the all plumes nominally firing case, the CFD modeling errors were estimated using the available OVERFLOW and LOCI-CHEM perfect gas solutions for the BDM #10 out case with an additional 30% margin to account for CFD validation errors. Available CFD solutions for off-nominal conditions (variations in attitude for fixed Mach and variations in Mach for fixed altitude) were used to estimate variations due to off-nominal flight conditions by subtracting the BDM-out database (nominal) increments from the corresponding off-nominal values. The maximum absolute values of the differences were set as the dispersion bounds to account for off-nominal flight conditions.

USM-out dispersions: The USM-out dispersion bounds consisted of three components, CFD modeling errors, variations due to α , β , $\Delta\alpha$, and $\Delta\beta$, and off-nominal flight conditions. The CFD modeling errors and variations due to off-nominal conditions were estimated using the same approach as the corresponding BDM-out dispersions. The dispersions due to α , β , $\Delta\alpha$ and $\Delta\beta$ were estimated using available CFD solutions for $\alpha = \beta = 4$ and were root-sum-squared with variations due to off-nominal conditions to obtain a combined dispersion bound independently dispersed with the dispersion bound for CFD modeling errors.

E. Database Implementation

The total aerodynamic coefficients for the upper stage and the first stage were obtained by summing up the free-stream coefficients, power-off increments, all plumes nominally firing increments, and, if applicable, one BDM-out or USM-out increments with associated uncertainty/dispersions. The free-stream coefficients and the power-off and power-on incremental coefficients were nondimensionalized by the free-stream dynamic pressure. However, the one BDM-out and one USM-out incremental coefficients were based on the thrust of that BDM or USM as if it were firing at nominal conditions.

VI. Discussion

Figures 16 and 17 present the isolated (free-stream) coefficients of the upper stage and the first stage at Mach 5.5. Since the power-off stage separation database is too large, it is not possible to present data plots to cover the entire range of the all the independent variables. Therefore, a few selected plots are presented to illustrate the trends and variations of power-off increments. Figures 18 and 19 present the upper stage and first stage power-off incremental coefficients for $R_{sep}/D = 0$ and $\alpha = \beta = \Delta\alpha = \Delta\beta = 0$. All the incremental coefficients except for axial force were set to zero for both upper stage and first stage since they were small. Due to facility limitations, the data could not be obtained at $X_{sep}/D = 0$. However, its value at $X_{sep}/D = 0$ can be estimated as follows.

The axial force coefficient consists of two components, forebody coefficient (C_{AF}) and base drag coefficient (C_{Ab}). The upper stage axial force increment (ΔC_A) is the difference between the axial force coefficient in proximity and in freestream. Since the forebody components are essentially same in freestream and in proximity, ΔC_A is the difference in the base drag components.

The base drag is given by

$$C_{AB} = -C_{pB} (S_{us}/S_{ref})$$

Here, C_{pB} is the base pressure coefficient, S_{us} is the cross sectional area of the upper stage and S_{ref} is the reference area (cross sectional area of the RSRMV). For the freestream case, the base pressure coefficient ($C_{pB,\infty}$) is approximately given by $-1/M_\infty^2$. For $M_\infty = 5.5$, $C_{pB,\infty} = -0.033$. With $S_{us}/S_{ref} = 2.25$, $C_{AB} = 0.0743$. In proximity, when the two stage just separate ($X_{sep}/D = 0$), the base pressure can be assumed equal to the freestream pressure so that C_{pB} is zero [3]. Hence, in proximity, $C_{AB} = 0$. Then $\Delta C_A = -0.0743$, which is consistent with $\Delta C_A = -0.066$ at $X_{sep}/D = 0.1$. This approximate analysis indicates that there is no sharp discontinuity in ΔC_A at $X_{sep}/D = 0$. As the two stages move apart, the base flow gets established gradually, the base pressure starts falling below the freestream value and ΔC_A approaches zero.

For the first stage, a freestream pressure in the frontal (gap) area results in a small axial force coefficient, and hence a negative increment in axial force coefficient as shown in Figure 19. As the two stages move apart, the upper stage base flow (wake) gets established and ΔC_A starts increasing. However, it would take much larger separation distances (beyond $X_{sep}/D = 5.5$) for ΔC_A to approach zero.

Figure 20 presents another sample result for the first stage for $R_{sep}/D = 0.2$, $\alpha = \beta = \Delta\alpha = \Delta\beta = 0$. The axial force increment follows the same trend as in Figure 19. Due to radial offset ($R_{sep}/D = 0.2$), the normal force, pitching

moment, side force, and yawing moment increments are nonzero as shown. The data is presented only for $\kappa = 0, 30, 60$ and 90 deg to avoid clutter in the plot. Note that the flow pattern for this case has top/bottom anti-symmetry and right/left symmetry. Using this property, data for other values of κ can be inferred. For example, $\Delta C_M(\kappa = 150) = -\Delta C_M(\kappa = 30)$, $\Delta C_M(\kappa = 330) = \Delta C_M(\kappa = 30)$. For side force increments, $\Delta C_Y(\kappa = 150) = \Delta C_Y(\kappa = 30)$, $\Delta C_Y(\kappa = 330) = -\Delta C_Y(\kappa = 30)$. For pitching moment increments, same equations as normal force increments apply, and for yawing moment increments, same equations as the side force increments apply. The rolling moment increments are zero for this case.

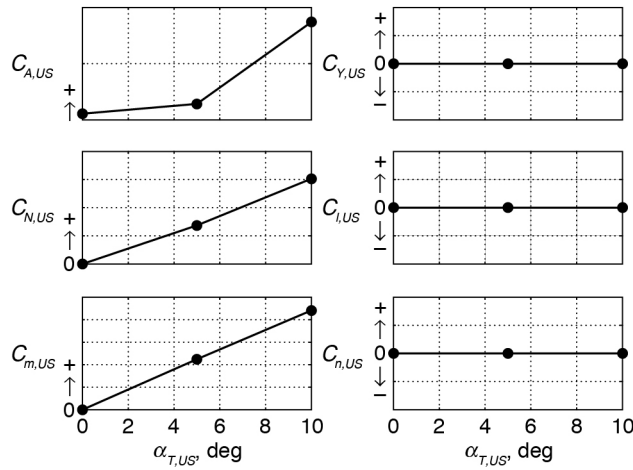


Fig. 16 Upper stage free-stream coefficients.

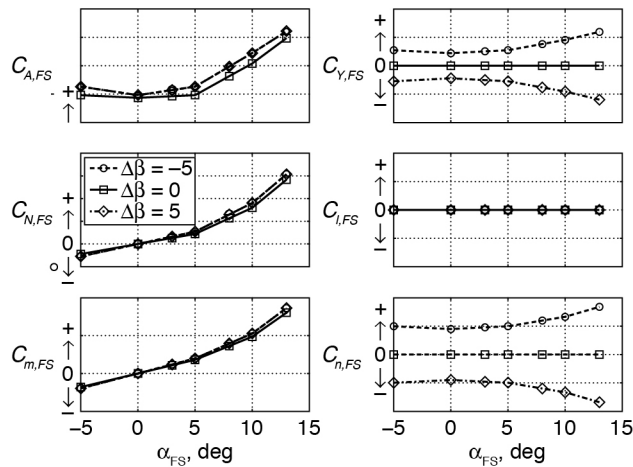


Fig. 17 First stage free-stream coefficients.

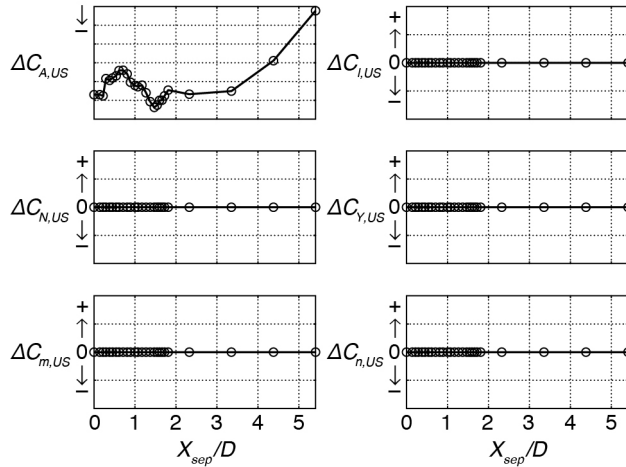


Fig. 18 Power-off upper stage incremental coefficients, $\alpha_{T, US} = 0$, $\Delta\alpha = 0$, $\Delta\beta = 0$, $R_{sep}/D = 0$.

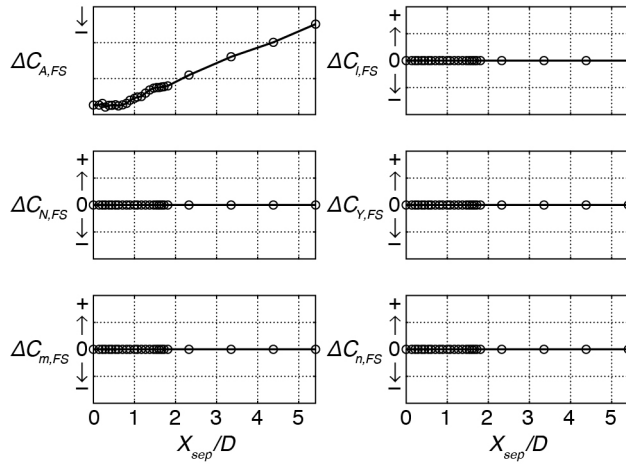


Fig. 19. Power-off first stage incremental coefficients, $\alpha_{T, US} = 0$, $\Delta\alpha = 0$, $\Delta\beta = 0$, $R_{sep}/D = 0$.

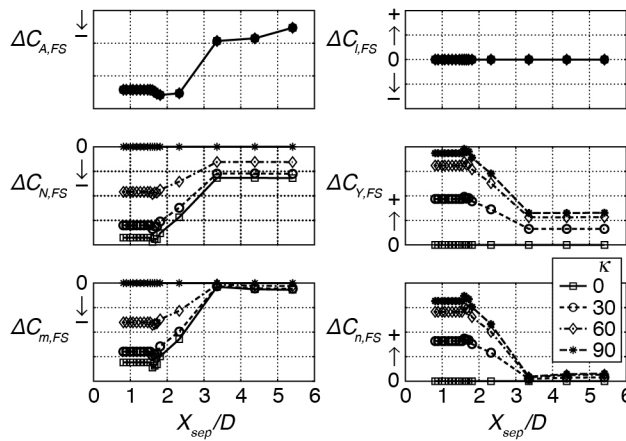


Fig. 20. Power-Off first stage incremental coefficients, $\alpha_{T, US} = 0$, $\Delta\alpha = 0$, $\Delta\beta = 0$, $R_{sep}/D = 0.2$.

Figure 21 shows the all plumes nominally firing axial force increments for upper stage, and Fig. 22 shows them for first stage. These increments were noted to be much larger than the corresponding power-off increments, particularly for the first stage. For $X_{sep}/D < 0.5$, the impingement pressure on the RSRMV kick rings (Fig. 9) due to BDM jets produces a thrust resulting in negative axial force increments. As X_{sep}/D increases, the pressurization of the first stage cup due to USM jets becomes significant and balances this thrust effect causing the incremental axial force coefficient to approach zero. For $X_{sep}/D > 2.5$, the J2-X thrust starts building up and impingement of the J2-X plume on the first stage cup produces positive axial force resulting in positive increments as observed in Figure 22.

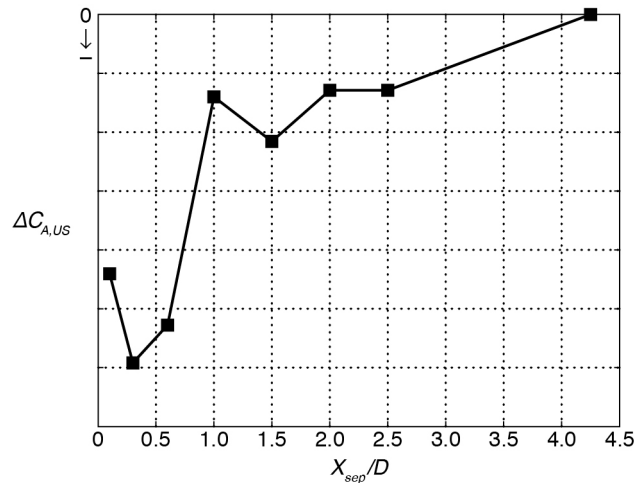


Fig. 21 Power-on upper stage axial force increments.

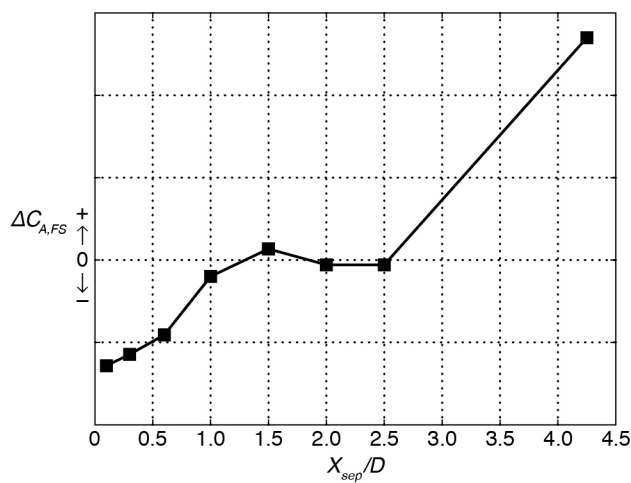


Fig. 22 Power-on first stage axial force increments.

Figure 23 shows one BDM-out force and moment increment coefficients (thrust based). It is observed that significant forces and moments resulted because of pressure imbalance on the first stage, particularly in the aft skirt region. For the BDM #10 failure, the pressures on the bottom side where its counterpart BDM #9 is firing are relatively higher. This pressure imbalance results in a large, positive normal force and an associated pitching moment. Similarly, when BDM #1 or #5 fail (not shown), a large side force and associated yawing moment arise. It was noted that these normal/side forces and associated pitching/yawing moments overwhelmed the all plumes nominally firing incremental forces/moments. As a result, the critical test for safe separation happens to be the one BDM failure case because these large increments in forces and moment further reduce the clearance between the first stage cup and the J2-X nozzle as the first stage cup tries to clear the J2-X nozzle (Fig. 6).

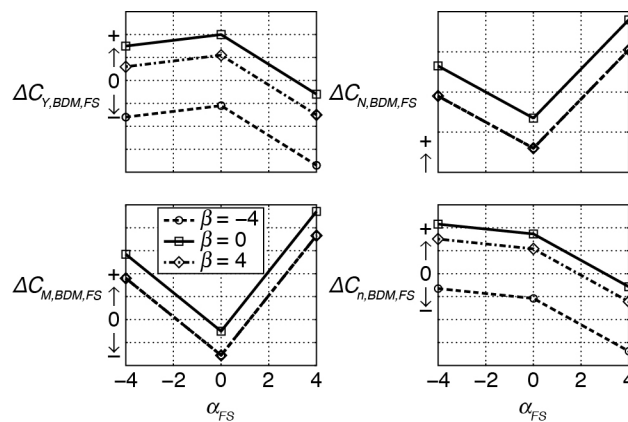


Fig. 23 BDM #10 Out first stage incremental coefficients.

Figure 24 shows one USM-out force and moment increment coefficients (thrust based) for upper stage, and Figure 25 shows them for first stage. These incremental coefficients are very small compared to BDM-out increments and may have negligible effect on separation clearance.

Figures 26 and 27 present sample results that show the dispersion bounds for power-on axial force increment coefficients for the upper stage and first stage. These dispersion bounds encompass all the residuals with extra margin except one point for first stage at $X_{sep}/D = 0.8$ as observed in Figure 27. This CFD data point was not used in developing the dispersion bounds but used as a check case. It was generated for limiting off-nominal conditions and falls within the worst-on-worst dispersion bounds.

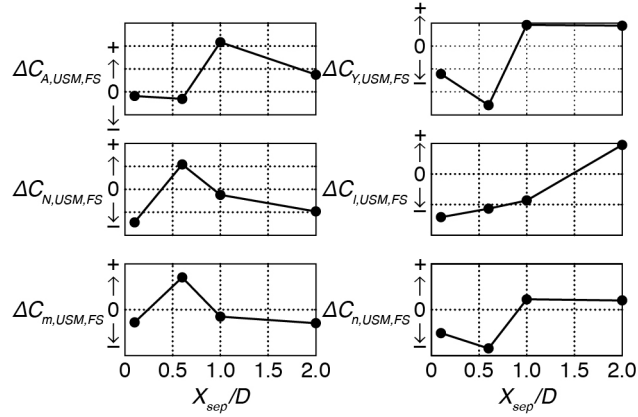


Fig. 24 USM #1 out upper stage incremental coefficients.

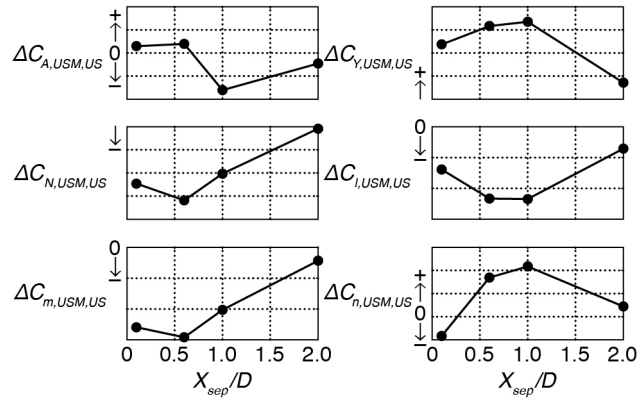


Fig. 25 USM #1 out first stage incremental coefficients.

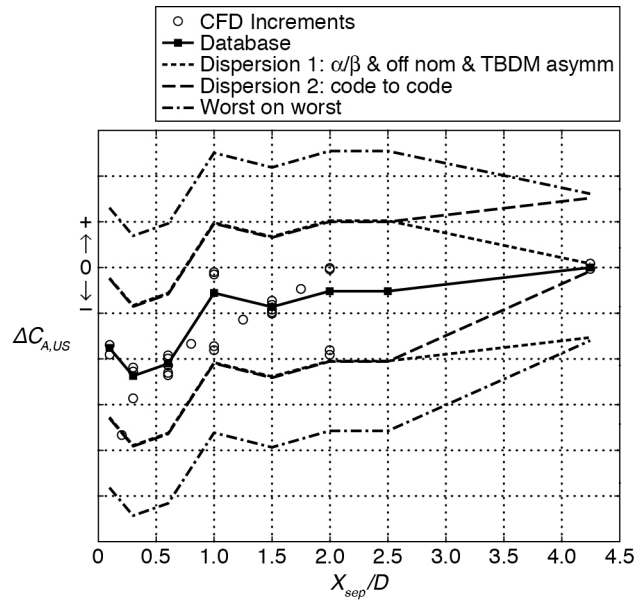


Fig. 26 Upper stage power-on incremental coefficient with dispersion bounds.

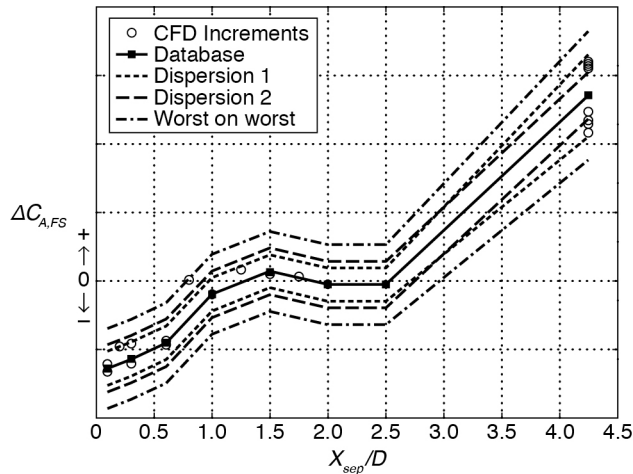


Fig. 27 First stage power-on incremental coefficient with dispersion bounds.

Concluding Remarks

The proximity aerodynamics during the Ares I A106 Crew Launch Vehicle stage separation is complex and challenging because of the presence of USM, BDM and J2-X plumes causing complex flow interactions in the upper stage base area and the first stage open cup region. It is a challenging task to design and fabricate powered test models because of the size limitations (typically 1% scale models) and to simulate all the plumes and obtain reliable test data for database development. Modern CFD tools offer a viable option but are expensive and difficult to validate without suitable test data. Conducting power-on tests was beyond the scope of this activity. In view of this, the approach taken was to perform power-off stage separation tests at AEDC VKF Tunnel A and use the OVERFLOW CFD code for estimating power-on increments.

The stage separation database consists of three components: freestream coefficients, power-off increments, and power-on increments. The database also consists of two additional components, one BDM-out and one USM-out incremental coefficients. The free-stream and power-off incremental databases were developed using stage separation test data. All the power-on incremental coefficients were estimated using OVERFLOW CFD solutions. It was observed that the power-on effects overwhelmed the power-off effects.

An estimated total of 130 air-on occupancy hours at AEDC VKF Tunnel A were needed for obtaining the requisite power-off stage separation test data. The limited power-on OVERFLOW CFD computations used in power-on database development, including BDM-out and USM-out cases, took about 35 million CPU hours on the Pleiades computer system at NASA Ames Research Center. In spite of using such a large number of CPU hours, it was not

possible to develop a suitable multi-dimensional power-on database. Simplified models were developed for the power-on database. All the parameters not modeled in the power-on database were included in developing the uncertainty. Since power-on OVERFLOW CFD solutions were not validated, additional margins had to be introduced that caused uncertainties to assume large values.

Acknowledgment

Les Hall, Michael Applebaum, Dr. Khaled S. Abdol-Hamid, Dr. Robert M. Hall, Dr. Michael J. Hensch and William G. Tomek are acknowledged for their help and assistance throughout the course of this activity.

References

¹Huebner, L. D., Haynes, D. A., Taylor, T. L., Hall, R. M., Pamadi, B. N., and Seaford, M. C., "Status, Plans, and Initial Results for Ares I Crew Launch Vehicle Aerodynamics," *Journal of British Interplanetary Society* (UK), Vol. 61, 2008.

²Pamadi, B. N., Pei, J., Covell, P. F., Favaregh, N. M., Gumbert, C. R., and Hanke J. L., "Aerodynamic Analyses and Database Development for Liftoff, Transition, and First Stage Ascent of the Ares I A106 Vehicle," AIAA Paper 2011-12, 49th AIAA Aerospace Sciences Meeting, Orlando, FL, January 2011.

³Nunley, B. W., "Static Aerodynamic Characteristics of the Apollo-Saturn IB Vehicle," NASA TM X-53657, September 25, 1967.

⁴Pinier, J. T. and Niskey, C. J., "Ares I and Ares I-X Stage Separation Aerodynamic Testing," AIAA Paper 2011-998, 49th AIAA Aerospace Sciences Meeting, Orlando, FL, January 2011.

⁵Nichols, R. H., Tramel, R. W., and Buning, P. G., "Solver and Turbulence Model Upgrades to OVERFLOW 2 for Unsteady and High-Speed Applications," AIAA-2006-2824, AIAA 36th Fluid Dynamics Conference, San Francisco, CA, June 2006.

⁶Hall, L., Applebaum, M. P., and Eppard, W. M., "Multi-Species Effects for Plume Modeling on Launch Vehicle Systems," AIAA-2011-1053, 49th AIAA Aerospace Sciences Meeting, Orlando, FL, January 2011.

⁷Smith, O. E., "A Reference Atmosphere for Patrick Air Force Base, Florida, Annual," NASA Technical Note D-595, March 1961.

⁸Klopfer, G. H., Onufer, J. T., Pandya, S. A., Chan, W. M., Kless, J. E., and Lee, H. C., "OVERFLOW Aerodynamic Predictions of the Ares I A106p Stage Separation Process with Viscous Plume Effects," NASA TM to be published.

⁹Chan, W. M., Gomez, R. J., Rogers, S. E., and Buning, P. G., "Best Practices in Overset Grid Generation," AIAA Paper 2002-3191, 2002.

¹⁰Lee, H. C., Klopfer, G. H., and Onufer, J. T., "OVERFLOW Validation for Predicting Plume Impingement of Under Expanded Axisymmetric Jets onto Angled Flat Plates," AIAA Paper 2011-1058, 49th AIAA Aerospace Sciences Meeting, Orlando, FL, January 2011.